Integrated Model for Resilience Evaluation of Power-gas Systems Under Windstorms

Yucui Wang, *Student Member*, *IEEE*, *Member*, *CSEE*, Yongbiao Yang, *Member*, *IEEE*, *Member*, *CSEE*, and Qingshan Xu, *Member*, *IEEE*, *Member*, *CSEE*

***Abstract*—Integrated power-gas systems (IPGS) have developed critical infrastructure in integrated energy systems. Moreover, various extreme weather events with low probability and high risk have seriously affected the stable operation of IPGSs. Due to close interconnectedness through coupling elements between the power system (PS) and natural gas system (NGS) when a disturbance happens in one system, a series of complicated sequences of dependent events may follow in another system. Especially under extreme conditions, this coupling can lead to a dramatic degradation of system performance, resulting in catastrophic failures. Therefore, there is an urgent need to model and evaluate resilience of IPGSs under extreme weather. Following this development trend, an integrated model for resilience evaluation of IPGS is proposed under extreme weather events focusing on windstorms. First, a framework of IPGS is proposed to describe states of the system at different stages under disaster conditions. Furthermore, an evaluation model considering cascading effects is used to quantify the impact of windstorms on NGS and PS. Meanwhile, a Monte Carlo simulation (MCS) technique is utilized to characterize chaotic fault of components. Moreover, time-dependent nodal and system resilience indices for IPGS are proposed to display impacts of windstorms. Numerical results on the IPGS test system demonstrate the proposed methods.**

***Index Terms*—Cascading effects, integrated power-gas systems, nodal resilience indices, optimal power flow model, resilience assessment, system resilience indices, windstorms.**

NOMENCLATURE

IPGS	Interdependent power and gas systems.
NGS	The natural gas system.
PS	The power system.
EDC	Electric-driven gas compressors.
GFGs	Gas-fired generators.
CFGs	Coal-fired generators.
MCS	Monte Carlo simulation.
IPCC	Intergovernmental Panel on Climate Change.
P2G	Power to gas.

Manuscript received August 7, 2022; revised November 6, 2022; accepted November 11, 2022. Date of online publication September 8, 2023; date of current version Feberuary 18, 2024. This work was supported by the Key Projects of National Natural Science Foundation of China (51936003).

Y. C. Wang is with the School of Cyber Science and Engineering, Southeast University, Nanjing 210096, China.

Y. B. Yang (corresponding author, email: 103200017@seu.edu.cn), and Q. S. Xu are with School of Electrical Engineering, Southeast University, Nanjing 210096, China; and also with Nanjing Center for Applied Mathematics, Nanjing 210096, China.

DOI: 10.17775/CSEEJPES.2022.05420

I. INTRODUCTION

THE energy crisis and environmental problems promote low-carbon transformation of the energy system and continuous optimization of the energy structure. Natural gas has been widely involved for its high efficiency and clean combustion products [1]. Moreover, rapid development of GFGspromotes coupling degrees of PS and NGS, making IPGS a typical form of integrated energy system [2].

As a result of the greenhouse effect, the probability of the world facing extreme disaster risk continues to increase [3], [4]. In recent decades, human beings have experienced about 400 extreme weather disasters every year. That is to say, one extreme weather disaster is staged every day in the world on average [5]. Particularly, the assessment report released by the IPCC in 2022 shows strong windstorms and extreme temperatures have increased and strengthened [6]. Under IPGS architecture, coordinated optimization of PS and NGS has improved energy utilization efficiency and promoted low-carbon transformation of the system. However, when a disturbance happens in one system, a series of complicated sequences of dependent events may follow in another system because of the close interconnectedness through the coupling elements, leading to catastrophic failure of the system [7], especially under extreme events. It is necessary to model and evaluate resilience of IPGSs under extreme weather.

Resilience is defined as the ability of systems to prevent and resist disturbances, recover to expected performance levels, and adapt to future catastrophic events when faced with small-probability and large-impact circumstances [8], [9]. Actually, some scholars have carried out resilience analysis for PS and NGS independently. Based on statistical methods, modeling and simulation techniques for power system resilience are proposed in [10]–[17]. An evaluation model is developed to discuss impact of tree trimming on power system resilience under hurricanes [10]. An advanced threats simulation technique is proposed in [11], in which a three-phase resilience analysis framework is developed at different stages during the hurricane period. An optimal power flow model to quantify power systems' resilience affected by severe windstorms utilized sequential MCS [12]. Reference [13] proposes a resilience assessment model considering fault propagation across regions to analyze performance of PS. Based on probabilistic modeling methods, a power system performance model is developed to estimate economic loss in the hurricane process [14]. Scholars have also researched resilience assessments of NGS under

extreme weather. Reference [15] presents a methodology based on resilience for assessing availability of NGS in the event of an earthquake. Recovery capacity of gas supply during severe weather conditions is discussed in [16]. A resilience evaluation model for the NGS is proposed in [17] based on the "electrical-thermal" uncertainty set. The above literature only studies independent PS or independent NGS, but ignores the coupling relationship between the two systems. However, with IPGS as a whole, faults can be propagated across regions by coupling components. So when one system suffers from extreme weather, the other is affected [18].

The above analysis shows PS and NGS interaction deserve attention. Scholars have widely recognized this view, and some studies on resilience evaluation of IPGS have been carried out [19], [22]. Coupling elements in the integrated distribution power system and NGS are energy hubs in [19], [20]. A resilience planning model based on multiple energy hubs is introduced to improve performance level of IPGS [19]. Reference [20] proposes a demand management strategy to ensure stable operation of IPGS under natural disasters. In addition, References [21] and [22] develop resilience assessment research on PS and NGS. A practical model is developed in [21] to evaluate load losses of IPGS. A resilience assessment model utilizing MCS reflects hurricane impacts on PS and NGS [22]. However, most previous studies use system-wide resilience indices to describe operating status under extreme weather without considering differences in nodes. Actually, due to different distributions of energy and demand, impact of severe weather on the system varies with different nodes. In addition, these indicators ignore the relationship with weather elements.

Moreover, previous studies on resilience evaluation of IPGS consider less the impacts of renewable energy. Actually, distributed energy resources account for an increasing proportion of power generation capacity, and damage degree of renewable energy equipment [23] is greatly related to weather conditions. Wind power generation is regarded as a substitute for conventional energy, which is an important part of an integrated energy system. Impacts of proportion of wind power generation brought to the IPGSs under windstorms will be discussed further in this paper.

To solve the above research gaps, this paper aims to propose a methodology to evaluate resilience of IPGSs considering cascading effects between PS and NGS under windstorms. The main contributions can be summarized as follows:

1) Time-dependent resilience assessment framework based on multi-phase performance response curve is proposed to evaluate IPGS performance levels under windstorms. There are four evaluation stages varying with performance of IPGS under windstorms. Furthermore, the MCS technique is employed to depict disorderly breakdown of elements.

2) An integrated model is proposed to evaluate resilience of IPGS, which represents the temporal and spatial process under windstorms considering cascading effects between NGS and PS. Moreover, impact of proportion of wind power generation on the IPGS resilience is discussed in this study.

3) Considering the impact of extreme weather on the system varies with different nodes, nodal resilience indicators are proposed. Indicators of expected energy loss, attenuation ratio, and recovery ratio are proposed to describe the expected level and instantaneous characteristics of resilience in IPGS. Further, these indicators consider the relationship with weather elements.

The rest of the paper is organized as follows. Time-dependent framework of resilience evaluation considering cascading effects between NGS and PS is proposed in Section II. Then, an integrated model for resilience assessment of IPGSs is represented in Section III. Section IV develops nodal resilience metrics of IPGSs. Section V verifies effectiveness of the proposed model and demonstrates simulation results. Conclusions are given in Section VI.

II. A Resilience Evaluation Framework Considering Cascading Effects of IPGS

A. Cascading Effects between NGS and PS

The IPGS is mainly composed of independent components and coupling components of NGS and PS, the architecture of which is shown in Fig. 1. Coupled elements realize bidirectional conversion of energy, including gas-fired combined heat and power units (CHPs), power to gas devices (P2Gs) and electricity-driven gas compressors (EDCs). Roles of coupling elements in PS and NGS are diametrically opposed, such as CHP being the energy consumer in NGS and energy supplier in PS. In contrast, P2Gs play the opposite role in NGS and PS, respectively. EDCs maintain gas pressure when sufficient electric energy is obtained. Specifically, P2G can only be turned on under wind energy abandonedment.

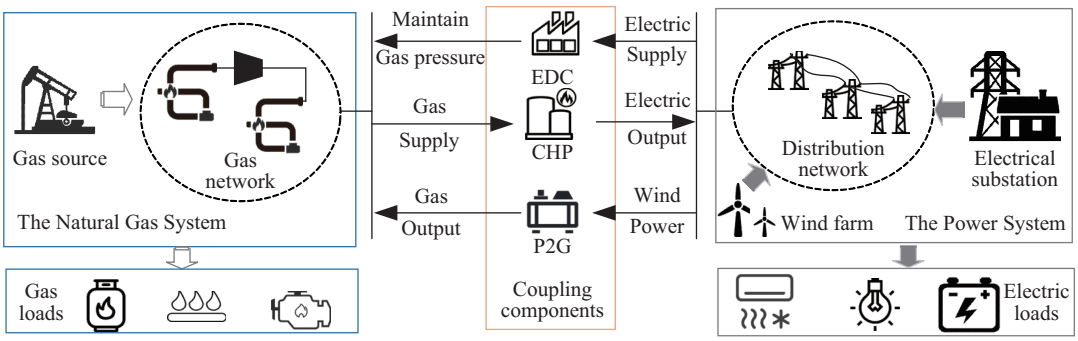

Fig. 1. Interdependent power-gas systems architecture.

When a system is subjected to extreme weather, such as windstorms, a disturbance happens in one system, then a series of complicated sequences of dependent events may follow in another system because of close interconnection through coupling elements, leading to catastrophic failure of the system [18]. In light of the fact pipelines in NGS are typically buried underground and, therefore, not subject to wind speed, it follows that windstorms primarily damage power system equipment. However, EDCs may experience reduced power supply during extreme weather events, as PS output may decrease. As a consequence, EDCs may cease functioning as a result of inadequate driving power supply. Under the circumstances, shortage of energy supply caused by extreme weather is spread to NGS. Besides, WTGs are sensitive to wind speed, which is likely to shut down in storm weather, affecting NGS through P2G. Further, gas supply to CHPs is reduced if gas supply is a shortage. Reduced output of CHPs exacerbates disequilibrium of PS. A vicious circle is formed due to interdependence of the two systems, leading to catastrophic failure of the system. The above is the description of the cascading process.

B. The Time-dependent Resilience Assessment Framework

The multi-phase performance response curve (shown in Fig. 2) is developed to assess IPGS performance levels under windstorms. The multi-phase performance response curve describes extreme events in four phases.

Phase I: Pre-disaster phase ($t \in [0, t_0)$) indicates the disaster prevention process from normal operation state to disaster failures. Performance of IPGS is at normal operation level before the meteorological disaster at t_0. In this phase, operators can make a meteorological prediction and formulate emergency plans.

Phase II: Resistance phase ($t \in [t_0, t_1)$) represents resistance of the IPGS to severe weather. During this period, operators schedule all available resources of the IPGS to maintain the system at a reliable operation level. However, under the influence of the disaster, there are component failures and derating in IPGS. As seen from Fig. 2, performance level of IPGS decreases to I at t_1.

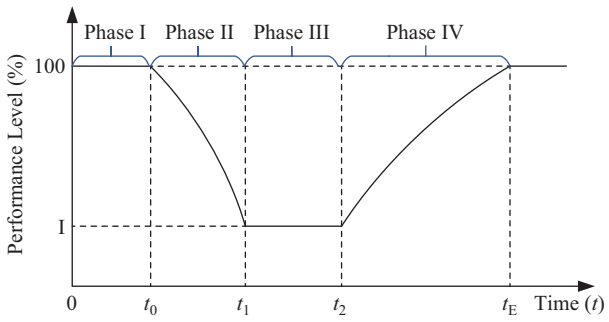

Fig. 2. Performance curve of IPGS under windstorms.

Phase III: Post-event phase ($t \in [t_1, t_2)$) reflects the time required to develop a recovery plan. It is necessary to make a repair plan for IPGS according to component types, fault sequences, and repair strategy. Therefore, the system maintains abnormal operation for some time.

Phase IV: Recovery phase ($t \in [t_2, t_E)$) refers to that after passage of extreme weather, the IPGS needs to be repaired. System performance is gradually restored as damaged components are repaired to normal levels. Recovery time depends on disaster degree and recovery ability of IGPS.

Time-dependent resilience assessment framework based on a multi-phase performance response curve is proposed, which is illustrated in Fig. 3. Impact of wind speeds on failures of components in IPGS is molded. Based on failure models of different elements, the systems' available state under windstorms is defined in the pre-disaster phase. Then, an optimal power flow model is proposed to schedule all available resources of IPGS in the resistance phase, considering cascading effects between PS and NGS. In order to restore the system to regular operation as soon as possible, a repair plan for IPGS is made in the post-event phase, and duration

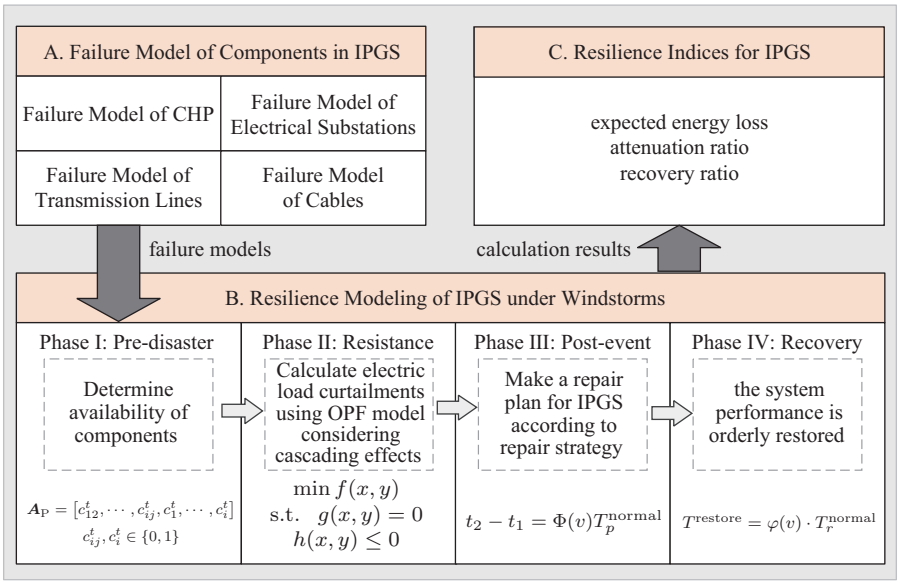

Fig. 3. Framework for resilience assessment of IPGS.

of this phase is determined by degree of component damage. System performance is restored orderly in the recovery phase according to the predetermined recovery plan in phase III. Finally, resilience indicators are proposed to describe the expected level and instantaneous characteristics of resilience in IPGS.

III. Integrated Model for Resilience Evaluating of IPGS under Windstorms

A. Failure Model of Components in IPGS

As the transmission system spans large areas and is exposed to the outdoor environment for a long time, it is susceptible to meteorological disasters. In contrast, the pipelines in the NGS are typically installed underground, so they are not subject to the effects of wind speed. Therefore, only windstorms that attack electrical components are considered in this study.

1) Failure Model of Electrical Substations

Substations are the main energy supply elements in PS and are a vital part of ensuring the safe and reliable operation of PS. The relationship between substation vulnerability and wind speed can be described as follows [24]:

$$p_i^{\mathrm{sub}}(v) = \phi\left(\frac{\ln(v)-\mu}{\sigma}\right) \tag{1}$$

where μ and σ are the logarithmic mean and the standard deviation, respectively, which are determined by the structural characteristics and layout of the substation [25]. The substation layout in this paper is a suburban substation, so the parameters μ and σ are 5.419 and 0.419, respectively.

2) Failure Model of CHPs

CHPs are divided into several types according to energy supply, including coal-fired units, gas-fired units, etc. In this paper, gas-fired CHPs are applied. The relationship between CHP failure probability and wind speed can be expressed as follows:

$$p_i^{\mathrm{G}}(v) = v\begin{cases} p_i^{\mathrm{G},0}, & \text{if } v \le v_{\mathrm{GI}} \\ p_i^{\mathrm{G},v}(v), & \text{if } v_{\mathrm{GI}} < v \le v_{\mathrm{GO}} \\ 1, & \text{if } v > v_{\mathrm{GO}} \end{cases} \tag{2}$$

where $p_i^{\mathrm{G}}(v)$ represents the function of CHPs failure probability varying with wind speed v; $p_i^{\mathrm{G},0}$ represents failure probability of CHPs under good weather conditions; $p_i^{\mathrm{G},v}(v)$ represents the relationship between the failure probability of CHPs and wind speed when wind speed is from v_{GI} to v_{GO}.

The fragility curve of CHPs is based on damage to building structures [23], as is the case for electrical substations. In the distribution network, buildings of substations [26] and CHP plants [27] are two-story concrete structures, which have the same fragility under windstorm attacks. Therefore, $p_i^{\mathrm{G},v}(v)$ is calculated by (1). v_{GI} and v_{GO} are 30 m/s and 45 m/s respectively.

3) Failure Model of Overhead Transmission Lines

Transmission line faults are most likely to occur under windstorms. Fault types are mainly divided into three categories: tripping caused by insulator flashover, tower collapses, and lines breaking. Fitting three types of faults [28], outage probability function of the line is as follows:

$$p_{ij}^{\mathrm{L}}(v) = \begin{cases} p_{ij}^{\mathrm{L},0}, & \text{if } v \le v_{\mathrm{LI}} \\ \exp\left[\frac{0.693(v-v_{\mathrm{LO}})}{v_{\mathrm{LO}}}\right]-1, & \text{if } v_{\mathrm{LI}} < v \le v_{\mathrm{LO}} \\ 1, & \text{if } v > v_{\mathrm{LO}} \end{cases} \tag{3}$$

where $p_{ij}^{\mathrm{L}}(v)$ represents the function of transmission lines failure probability varying with wind speed v; $p_{ij}^{\mathrm{L},0}$ represents failure probability of transmission lines under good weather conditions; v_{LI} represents maximum wind speed for normal operation of transmission line, $v_{\mathrm{LO}} = 2{\cdot}v_{\mathrm{LI}}$; failure probability is an exponential function of wind speed v when wind speed is from v_{LI} to v_{LO}.

4) Failure Model of Cables

Similar to pipelines in the NGS, cables are usually buried underground and are insensitive to wind speed. Hence, failure probability of cable under windstorms is equal to that under good weather, which is represented as:

$$p_{ij}^{\mathrm{C}}(v) = p_{ij}^{\mathrm{C},0} \tag{4}$$

where $p_{ij}^{\mathrm{C},0}$ is failure probability of cables under normal weather.

B. Integrated Model for Resilience Evaluating of IPGS under Windstorms

1) Phase: Pre-disaster Phase

Performance level of the system begins to decline at 0. Failure models of different components considering the impacts of windstorms on PS have been illustrated in the previous section. Vector $\boldsymbol{A}_{\mathrm{P}}$ is introduced to represent available status of various components of PS under windstorms.

Performance level of the system is a random combination of availability of various components, including CHPs, electrical substations, transmission lines and cables.

$$\boldsymbol{A}_{\mathrm{P}} = [c_{12}^t, c_{13}^t, \cdots, c_{ij}^t, c_1^t, c_2^t, \cdots, c_i^t] \tag{5}$$

$$c_{ij}^t, c_i^t \in \{0,1\} \tag{6}$$

where c_{ij}^t represents operating state of overhead transmission line ij or cable ij at time t; c_i^t represents operating state of CHPs or electrical substations.

Value of elements in $\boldsymbol{A}_{\mathrm{P}}$ is either 1 or 0, where 1 represents normal operating state of power components, and 0 represents failure operating state. It is worth noting operating condition of component at time t depends on the previous time. Moreover, failure of components is random. The MCS technique is utilized to characterize randomness of component failure. Taking the CHP i as an example, its operation state c_i^t at time t is based on current failure probability and previous operating condition utilizing the CMS technique [29].

$$c_i^t = \begin{cases} c_i^{t-1}\cdot 1, & \text{if } p_i^{\mathrm{G}}(v) \le r \\ c_i^{t-1}\cdot 0, & \text{if } p_i^{\mathrm{G}}(v) > r \end{cases} \tag{7}$$

where r is a random number and $r \in (0,1)$. Value of r is independent of wind speed, while value $p_i^{\mathrm{G}}(v)$ reflects influence of wind speed on the CHP.

2) Phase II: Resistance Phase

Under IPGS architecture, coordinated optimization of PS and NGS has improved energy utilization efficiency and promoted low-carbon transformation of the system. However, when a disturbance happens in one system, a series of complicated sequences of dependent events may follow in another system because they are closely interconnected through coupling elements. Moreover, since windstorms attack IPGS at the time t_0, components are in chaotic faults, which makes the system out of its normal operation state. In order to maintain the system at a reliable operation level, an optimal power flow model is proposed to schedule all available resources of the IPGS, which considers cascading effects between PS and NGS.

Objective function: Performance level of IPGS decreases to I at t_1, shown in Fig. 2. To reduce impact of windstorms, the objective function is to minimize total costs of load reduction, which is expressed as:

$$\min f = \sum_{m=1}^{\mathrm{M}} \sum_{t=0}^{t_E} (c_{\mathrm{P}} \cdot L_{\mathrm{C},m}^{t}) + \sum_{i=1}^{\mathrm{N}} \sum_{t=0}^{t_E} (c_{\mathrm{G}} \cdot L_{\mathrm{GC},i}^{t}) \tag{8}$$

where $L_{\mathrm{C},m}^{t}$ and c_{P} are power load curtailment and cost coefficient at node m for time t, respectively. $L_{\mathrm{GC},m}^{t}$ and c_{G} are gas load curtailment and cost coefficient at node i for time t.

PS and NGS are subject to the following constraints.

PS constraints:

Gas-fired CHPs: Working modes of CHP are divided into mode of determining electricity by heat and mode of determining heat by electricity. This paper focuses on energy supply of PS and NGS under extreme weather instead of energy-related services. Therefore, thermal output of CHP is ignored in this paper. Output of a CHP at the installed electric node m and corresponding gas flow obtained from gas node i can be denoted as:

$$P_{\mathrm{CHP},m}^{t} = \eta_E \cdot \psi \cdot S_{\mathrm{G},i}^{t} \tag{9}$$

$$c_{\mathrm{CHP},i}^{t} \cdot P_{\mathrm{CHP},m}^{\min,t} \le P_{\mathrm{CHP},m}^{t} \le c_{\mathrm{CHP},i}^{t} \cdot P_{\mathrm{CHP},m}^{\max,t} \tag{10}$$

where η_E and ψ are electrical efficiency of CHP and gas gross heating value. $c_{\mathrm{CHP},i}^{t}$ is availability coefficient of CHP at time t, which is defined in matrix $\boldsymbol{A}_{\mathrm{P}}$. $P_{\mathrm{CHP},m}^{\min,t}$ and $P_{\mathrm{CHP},m}^{\max,t}$ are minimum output and maximum output of CHP at bus m. $S_{\mathrm{G},i}^{t}$ is gas injection at gas node i for time t, which is defined as:

$$S_{\mathrm{G},i}^{t} = W_{i}^{t} - L_{\mathrm{GC},i}^{t} \tag{11}$$

Wind turbine generators: Wind energy is regarded as one of the most potential primary energy sources and is widely used in power generation. Output of WTGs varies with wind speed, which is expressed as:

$$P_{\mathrm{WTG},m}^{t} = \begin{cases} 0, & \text{if } 0 \le v^t < v_{\mathrm{ci}}^t, v^t \ge v_{\mathrm{co}}^t \\ P_{\mathrm{WTG}}^{\mathrm{r}} \frac{v - v_{\mathrm{ci}}}{v_r - v_{\mathrm{ci}}}, & \text{if } v_{\mathrm{ci}}^t \le v^t < v_{\mathrm{r}}^t \\ P_{\mathrm{WTG}}^{\mathrm{r}}, & \text{if } v_{\mathrm{r}}^t \le v^t < v_{\mathrm{co}}^t \end{cases} \tag{12}$$

where v^t is wind speed, which is obtained by Weibull function; v_{ci}^t, v_{co}^t, and v_{r}^t are cut-in speed, cut-out speed, and rated speed at time t, respectively; $P_{\mathrm{WTG}}^{\mathrm{r}}$ is rated power of WTG.

To avoid permanent damage to the WTGs, cut-out wind speed is set to 19∼25 m/s [30]. When wind speed exceeds cut-out wind speed, the unit stops.

Line flow: In order to make the proposed evaluation model applicable, linearized AC power flow model [31] is utilized. Reference [31] proves the introduced error is acceptable under normal and extreme weather conditions. Detailed proof process is given in [31].

$$k_{mn\_1} = \frac{x_{mn}}{r_{mn}^2 + x_{mn}^2}, \quad k_{mn\_2} = \frac{r_{mn}}{r_{mn}^2 + x_{mn}^2} \tag{13}$$

$$P_{mn}^{t} = k_{mn\_1}(\delta_m^t - \delta_n^t) + k_{mn\_2}(V_m^t - V_n^t) \tag{14}$$

$$Q_{mn}^{t} = -k_{mn\_2}(\delta_m^t - \delta_n^t) + k_{mn\_1}(V_m^t - V_n^t) \tag{15}$$

$$P_{m}^{t} = \sum_{m=1, m\ne n}^{M} k_{mn\_1}(\delta_m^t - \delta_n^t) + k_{mn\_2}(V_m^t - V_n^t) \tag{16}$$

$$Q_{m}^{t} = \sum_{m=1, m\ne n}^{M} -k_{mn\_2}(\delta_m^t - \delta_n^t) + k_{mn\_1}(V_m^t - V_n^t) \tag{17}$$

$$|P_{mn}^{t}| \le P_{mn}^{\max,t} \tag{18}$$

$$|Q_{mn}^{t}| \le Q_{mn}^{\max,t} \tag{19}$$

where x_{mn} and r_{mn} are reactance and resistance of branch mn. δ_m^t and V_m^t are voltage angle and voltage magnitudes at electric node m. $P_{mn}^{\max,t}$ and $Q_{mn}^{\max,t}$ are maximum active power and maximum reactive power between node m and n.

Power flow balance on each node: Power inflow and outflow of electric node m are dynamically balanced at each node, which is described as:

$$P_{\mathrm{CHP},m}^{t} + P_{\mathrm{WTG},m}^{t} - (L_{\mathrm{load},m}^{t} - L_{\mathrm{C},m}^{t}) + \sum_{m\in\Omega_{\mathrm{in}}^{t}} P_{1,m}^{t} - \sum_{m\in\Omega_{\mathrm{out}}^{t}} P_{1,m}^{t} = 0 \tag{20}$$

$$Q_{\mathrm{CHP},m}^{t} + Q_{\mathrm{WTG},m}^{t} - (L_{\mathrm{load},m}^{\mathrm{Q},t} - L_{\mathrm{CQ},m}^{t}) + \sum_{m\in\Theta_{\mathrm{in}}^{t}} Q_{1,m}^{t} - \sum_{m\in\Theta_{\mathrm{out}}^{t}} Q_{1,m}^{t} = 0 \tag{21}$$

where $P_{\mathrm{CHP},m}$ and $Q_{\mathrm{CHP},m}$ are active and reactive output of CHPs at electric node m; $L_{\mathrm{load},m}^{t}$ and $L_{\mathrm{load},m}^{\mathrm{Q},t}$ are active power load and reactive power load at time t; Ω_{in}^{l} and Θ_{in}^{l} are sets of power lines with incoming node being power node m; $\Omega_{\mathrm{out}}^{l}$ and $\Theta_{\mathrm{out}}^{l}$ are sets of power lines with outgoing node being power node m.

Natural system constraints:

Non-electric-driven compressor: Performance of compressor is mainly reflected by compression ratio R_{nedc}^{t}, which is expressed as:

$$R_{\mathrm{nedc},i}^{t} = \frac{\pi_{\mathrm{I}}^{t}}{\pi_{\mathrm{O}}^{t}} \tag{22}$$

$$R_{\mathrm{nedc},i}^{\min,t} \cdot \pi_{\mathrm{O}}^{t} \le \pi_{\mathrm{I}}^{t} \le R_{\mathrm{nedc},i}^{\max,t} \cdot \pi_{\mathrm{O}}^{t} \tag{23}$$

$$R_{\mathrm{nedc},i}^{\min,t} \le R_{\mathrm{nedc},i}^{t} \le R_{\mathrm{nedc},i}^{\max,t} \tag{24}$$

where $R_{\mathrm{nedc},i}^{t}$ is compressor ratio at time t; π_{I}^{t} and π_{O}^{t} are gas pressure of incoming node and outgoing node, respectively.

Electric-driven compressor: EDC is the coupling element between NGS and PS. Power $P_{\mathrm{edc},m}^{t}$ consumed by EDC

depends on its compression ratio R^t_{edc}, and operating status of EDC is affected not only by its characteristics but also by power supply, which can be represented as:

$$P^t_{\mathrm{edc},m} = \eta_{\mathrm{edc}} \cdot R^t_{\mathrm{edc},i}$$

$$O^t_{\mathrm{edc},i} = \begin{cases} 1, & \text{if } P^t_{\mathrm{edc},m} \le L^t_m - L^t_{\mathrm{C},m} \\ 0, & \text{if } P^t_{\mathrm{edc},m} > L^t_m - L^t_{\mathrm{C},m} \end{cases} \tag{25}$$

$$O^t_{\mathrm{edc},i} R^{\min,t}_{\mathrm{edc},i} \le R^t_{\mathrm{edc},i} \le O^t_{\mathrm{edc},i} R^{\max,t}_{\mathrm{edc},i} \tag{26}$$

where η_{edc} is conversion factor; $O^t_{\mathrm{edc},i}$ is running condition coefficient, $O^t_{\mathrm{edc},i} = 1$ when EDC gain sufficient electric supply, otherwise $O^t_{\mathrm{edc},i} = 0$. $R^{\min,t}_{\mathrm{edc},i}$ and $R^{\max,t}_{\mathrm{edc},i}$ are minimum compression ratio and maximum compression ratio of the EDC at time t.

Gas source: Output of the gas source is bounded by:

$$W^{\min,t}_{\mathrm{gs},i} \le W^t_{\mathrm{gs},i} \le W^{\max,t}_{\mathrm{gs},i} \tag{27}$$

where $W^{\min,t}_{\mathrm{gs},i}$ and $W^{\max,t}_{\mathrm{gs},i}$ are minimum output and maximum output of the output of gas source.

Power to gas: P2G is a vital coupling device in IPGS. Generally, it cooperates with renewable energy power generation to convert abandoned energy into gas energy. Moreover, wind power is regarded as a substitute for conventional energy, providing the possibility for large-scale development of wind power after complementing the P2G technique. P2G can only be turned on when wind energy is abandoned in this study.

The model of P2G is defined as:

$$W^t_{\mathrm{P2G},i} = \begin{cases} \frac{\eta_{\mathrm{P2G}} \cdot P^t_{\mathrm{P2G},m,}}{\mathrm{GHV}}, & \sum_{z=1}^{N_{\mathrm{WTG}}} \Delta P^{t,z}_{\mathrm{WTG},m} > 0 \\ 0, & \sum_{z=1}^{N_{\mathrm{WTG}}} \Delta P^{t,z}_{\mathrm{WTG},m} = 0 \end{cases} \tag{28}$$

where η_{P2G} is conversion efficiency of P2G device; $W^t_{\mathrm{P2G},i}$ and $P^t_{\mathrm{P2G},m}$ are gas production and electric power consumption at gas node i, respectively; $\Delta P^{t,z}_{\mathrm{WTG},m}$ is wind abandonment at electric node m; there are N_{WTG} WTGs.

Gas flow: Weymouth equation is one of the main ways to solve gas flow [32]. Gas flow of each pipeline is defined as:

$$f^t_{\mathrm{pl}} |f^t_{\mathrm{pl}}| = \Psi_{\mathrm{pl}} (\pi^t_{\mathrm{pl},f} - \pi^t_{\mathrm{pl},t}) \tag{29}$$

where f^t_{pl} is gas flow at time t; $\pi^t_{\mathrm{pl},f}$ and $\pi^t_{\mathrm{pl},t}$ are squared pressure of the "from" node and the "to" node; Ψ_{pl} is Weymouth constant coefficient.

It can be seen that (29) is nonlinear, which brings difficulty to solution of the model. Therefore, piecewise linearization techniques are used to linearize it, and specific details are in [12].

Gas flow balance on each node: Incoming gas flow is in balance with outgoing gas flow at node j for time t.

$$W^t_{\mathrm{gs},i} + W^t_{\mathrm{P2G},i} - \left(L^{\mathrm{G},t}_{\mathrm{load},i} - L^t_{\mathrm{GC},i}\right) + \sum_{i \in \Omega^{\mathrm{p}}_{\mathrm{in}}} f^t_i - \sum_{i \in \Omega^{\mathrm{pl}}_{\mathrm{out}}} f^t_i = 0 \tag{30}$$

where $L^{\mathrm{G},t}_{\mathrm{load},i}$ is gas load; $\Omega^{\mathrm{pl}}_{\mathrm{in}}$ is set of gas pipelines pl with gas node i as incoming node; $\Omega^{\mathrm{pl}}_{\mathrm{out}}$ is set of gas pipelines pl with gas node i as the outgoing node.

3) Phase III: Post-event Phase

Operators make a repair plan for IPGS according to component types, faults sequences and repair strategy in Phases III. Besides, repair resources are allocated according to repair policy. Duration of this phase $(t_2 - t_1)$ is closely related to how damaged the component is [33]. The higher the wind speed, the longer it takes to make a plan, which is represented as:

$$t_2 - t_1 = \Phi(v) T^{\mathrm{normal}}_{\mathrm{p}} \tag{31}$$

where $T^{\mathrm{normal}}_{\mathrm{p}}$ is mean time spent to make plan under good weather, which is assumed to be 3 h [12]. $\Phi(v)$ is a factor that represents windstorms intensity and duration.

4) Phase IV: Recovery Phase

According to the recovery plan in phase III, repair measures for IPGS are taken at t_2. There are some assumptions: (i) In consideration of security factors, maintenance crews are dispatched only in the recovery phase. (ii) Once all damaged components are repaired, the system can resume operation. (iii) Duration of the crews transferring from one maintenance point to another can be neglected.

Although each component is indispensable in IPGS, impact on the system varies when component is damaged. For example, failure of generators or lines connected to them often leads to a large-area power interruption, while line break at the edge of the system only causes load curtailment at one node. Therefore, based on the predetermined recovery plan, system performance is orderly restored in this phase. In this paper, specific description of repair policy is when the number of crews is insufficient to repair all failed components at the same time, components that have a significant impact on safe operation of PS are repaired first, such as generators. The smaller the impact of component damage on PS, the later the repair time. Repair crews spent more time restoring damaged elements for higher wind speeds [13], which is expressed as:

$$T^{\mathrm{restore}} = \varphi(v) \cdot T^{\mathrm{normal}}_{\mathrm{r}} \tag{32}$$

where T^{restore} is restoration time for damaged components; $T^{\mathrm{normal}}_{\mathrm{r}}$ is mean time to repair under good weather; $\varphi(v)$ is operator that describes the correlation between intensity of windstorms and the duration required for repair, and specific expression is represented as [13]:

$$\varphi(v) = 1 + \varepsilon \cdot (v_{\mathrm{wind}} - v_{\mathrm{crit}}) \tag{33}$$

where ε is a positive parameter and is set to 0.4 based on engineering common sense; v_{wind} is wind speed of the windstorm; v_{crit} is critical wind speed and is set to 8 m/s [13].

IV. Resilience Indices for IPGS

A. Resilience Indices for IPGS

Resilience of the system refers to the ability to resist, absorb and recover from extreme disasters. For the three aspects, indicators of expected energy loss, attenuation ratio and recovery ratio are proposed to describe expected level and instantaneous characteristics of resilience in IPGS. Further, these indicators consider the relationship with weather intensity.

Performance loss: Nodal expected electricity energy loss $L_{\mathrm{EE},m}$ and nodal expected gas energy loss $L_{\mathrm{GE},i}$ reflect average resilience level of the IPGS, which are represented as:

$$L_{\mathrm{EE},m} = \sum_{s=1}^{S}\left[\sum_{k=0}^{t_E/\Delta t}\left(\frac{L_{\mathrm{C},m}^{k\cdot\Delta t}}{L_m^0}\right)\cdot\frac{\Delta t}{t_E}\right]\Big/S \tag{34}$$

$$L_{\mathrm{GE},i} = \sum_{s=1}^{S}\left[\sum_{k=0}^{t_E/\Delta t}\left(\frac{L_{\mathrm{GC},i}^{k\cdot\Delta t}}{L_{\mathrm{G},i}^0}\right)\cdot\frac{\Delta t}{t_E}\right]\Big/S \tag{35}$$

where Δt is time interval for re-evaluation of IPGS resilience, which is assumed as 1 h; b is total number of time intervals, equal to $t_E/\Delta t$; S is total simulation times of MCS.

Attenuation ratio: Attenuation ratio R_A represents instantaneous resilience of IPGS, which describes how quickly IPGS performance level declines in resistance phase.

$$R_A = \sum_{s=1}^{S} \cdot\left[\sum_{b=1}^{(t_1-t_0)/\Delta t}\frac{\sum_{i=1}^{N}\left(\Delta P_i^{t_0+(b-1)\cdot\Delta t}-\Delta P_i^{t_0+b\cdot\Delta t}\right)/\Delta t}{(t_1-t_0)/\Delta t}\right]\Big/S \tag{36}$$

where ΔP_i is performance variation of node i, that is change of expected energy loss.

Recovery ratio: Recovery ratio R_R is also an instantaneous indicator, which represents ability of IPGS to return to its initial state after encountering extreme weather in recovery phase.

$$R_R = \sum_{s=1}^{S} \cdot\left[\sum_{b=1}^{(t_1-t_0)/\Delta t}\frac{\sum_{i=1}^{N}\left(\Delta P_i^{t_2+b\cdot\Delta t}-\Delta P_i^{t_2+(b-1)\cdot\Delta t}\right)/\Delta t}{(t_E-t_2)/\Delta t}\right]\Big/S \tag{37}$$

Based on nodal resilience indicators, system indicators are represented as:

$$L_{\mathrm{EE}} = \sum_{s=1}^{S}\left[\sum_{k=0}^{t_E/\Delta t}\sum_{m=1}^{M}\left(\frac{L_{\mathrm{C},m}^{k\cdot\Delta t}}{L_m^0}\right)\frac{\Delta t}{t_E}\right]\Big/S \tag{38}$$

$$L_{\mathrm{GE}} = \sum_{s=1}^{S}\left[\sum_{k=0}^{t_E/\Delta t}\sum_{i=1}^{N}\left(\frac{L_{\mathrm{GE},i}^{k\cdot\Delta t}}{L_{gi}^0}\right)\frac{\Delta t}{t_E}\right]\Big/S \tag{39}$$

B. Calculation Procedures

As shown in Fig. 4, procedures for resilience evaluation of IGPSs can be divided into three steps. First step is to initialize component parameters and states to obtain initial operational state of the IPGS.

Second step is resilience assessment of IGPS based on MCS techniques. This process is a simulation from 0 to t_E, with Δt simulation step. Four phases illustrated in Section III are included in this step: availability probability of components is determined utilizing CMS technique in phase; energy supply levels are gained by optimal energy flow model described in (8)–(30) in phase II; repair plan and strategies are given in phase III and IV, respectively. Repeat previous procedures until stopping criterion for the MCS technique is satisfied. Stopping criterion is defined as:

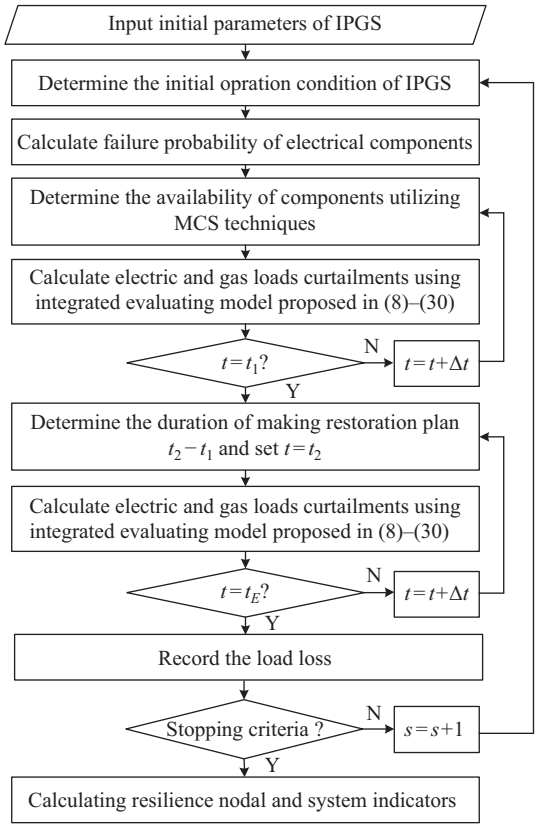

Fig. 4. Procedures of resilience evaluation.

$$\eta = \max\left(\sqrt{V(L_{\mathrm{EE}})}/L_{\mathrm{EE}}, \sqrt{V(L_{\mathrm{GE}})}/L_{\mathrm{GE}}\right) \tag{40}$$

where $V(\cdot)$ is variance.

Third step is to calculate nodal and system resilience indicators using results of optimal energy flow model.

V. Case Studies

An integrated IEEE 33-bus power system [34] and Belgian 20-node gas system [35] form an IPGS, as shown in Fig. 5. PS contains two CHPs contain (G1 and G2), and one WTG (G3). Lines 1–2, 5–4, 5–6, 13–12, and 13–14 are assumed as underground cables. In the NGS, there are three compressors, two of which are electric-driven (C2 and C3). There are three gas sources (W1, W2, and W3) and 1 P2G facility in the NGS. Specific location of components and energy supply path to EDCs and CHPs are shown in Fig. 5. Reference [36] gives detailed parameters of compressors and pipelines. Electrical efficiency of CHP is set as 0.5. Heat rate coefficients of CHPs are represented in [37]. Conversion coefficient of P2G is set as 0.09 m^3/KW. Interruption cost of customers in PS is set as 2000 \$/MW.

Assuming the storm starts attacking the system at 10 h, duration of this process is 12 h ($t_1 - t_0 = 12$ h). Time interval for resilience re-evaluation is one hour. Restoration time for

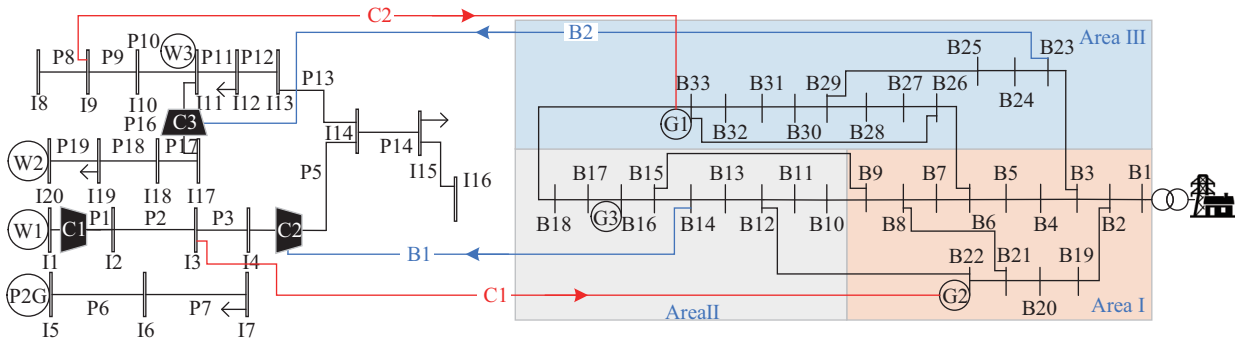

Fig. 5. Test integrated power-gas systems.

damaged lines, CHPs, and electrical substations under normal weather is 2 h, 4 h, and 8 h. Wind speeds consider 31 m/s, 36 m/s, and 41 m/s based on windstorm classification [12]. Corresponding failure probabilities of overhead lines at wind speeds of 31 m/s, 36 m/s and 41 m/s are 0.05, 0.10 and 0.20, respectively [28]. Operator $\Phi(v)$ and $\varphi(v)$ are determined by uniform sampling; sampling range of which is [2], [3] for $30 \leq v \leq 40$ and [3], [4] for higher wind speeds [24].

Formulation of the reliability evaluation is accomplished by MATLAB R2020b and Gurobi 9.1.2. The above software is installed on a personal computer with Intel 1.8 GHz 4-core processor and 8 GB memory.

There are three cases to assess resilience of IPGS.

Case 1: IPGS maintains original data. Resilience of IPGS is evaluated under wide grid-scale windstorms (wind speed in the test system is the same) with 31 m/s, 36 m/s, and 41 m/s wind speeds.

Case 2: There are three scenarios depending on degree of coupling.

Scenario A: Scenario A is the same as *Case 1*.

Scenario B: CHPs is fueled by external gas sources instead of NGS. The rest are the same as *Case 1*.

Scenario C: CHPs is fueled by external gas sources instead of the NGS. EDCs obtain power supply from an external power device.

Case 3: PS is randomly divided into three areas, as shown in Fig. 5. Assuming windstorms only attack one of the systems. Wind speed under normal weather conditions is 20 m/s.

Case 4: The difference from *Case 1* is that WTGs of the same capacity replace CHPs in turn.

A. The Impacts of Coupling Degree on Resilience Evaluation of IPGS

In order to examine influence of coupling degree on system resilience, we analyze and compare assessment outcomes of *Case 2*.

Cascading between PS and NGS is realized through coupling elements, which have been described in Section II-A. Therefore, the number of coupling elements reflects coupling degree. Coupling elements include gas-fired CHPs and EDCs.

When CHP obtains gas supply from outside, CHP does not play a role of connecting the two systems, so it is an uncoupling element. Similarly, when EDC obtains power from outside, it is an uncoupling component. Based on the above analysis, the number of coupling elements of *Scenarios A, B* and *C* is 4, 2 and 0, respectively. Energy supply levels for different coupling degrees are shown in Fig. 6, and ranking of nodal resilience indices is shown in Fig. 7.

Obviously, the trend of the curve in Fig. 6 is similar to Fig. 2. Besides, regarding power supply levels above Fig. 6(a), the higher the wind speed, the lower the maximum power

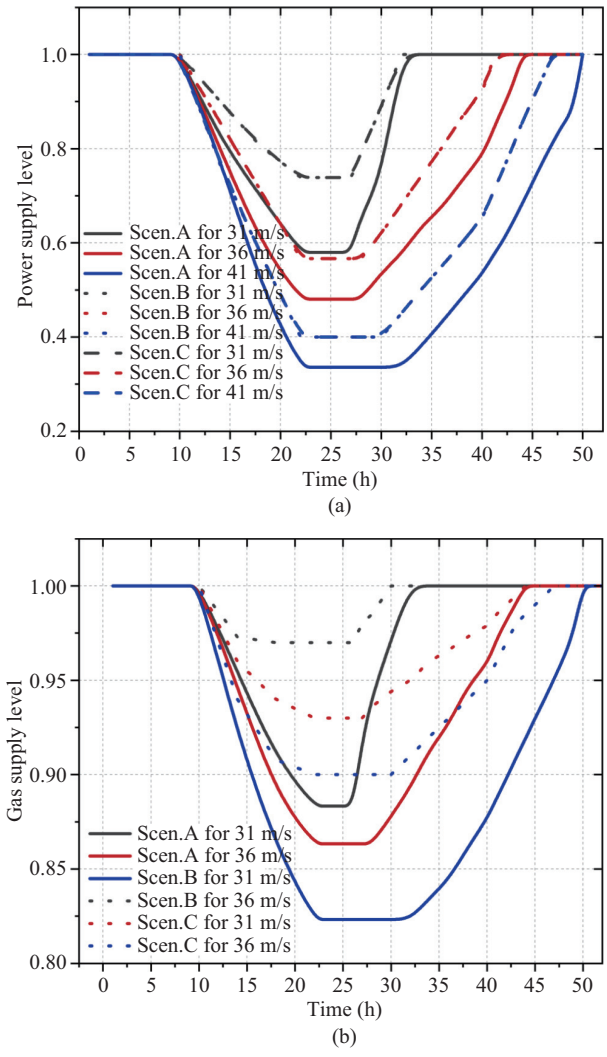

Fig. 6. Energy supply levels for different coupling degree. (a) Power supply level for IPGS and IPS. (b) Gas supply level for IPGS.

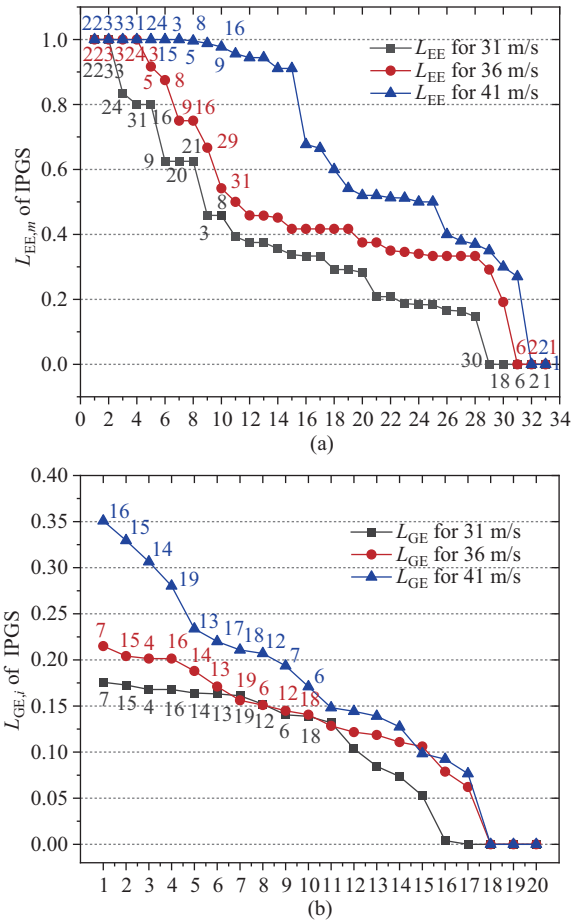

Fig. 7. Ranking of nodal resilience indices for Scenario A (Case 1). (a) Ranking of nodal resilience indices in PS. (b) Ranking of nodal resilience indices in NGS.

supply level after the windstorms attack (at 22 h) mostly for IPGS and independent power system (IPS), respectively. The reason for this is that destructive force of the windstorm grows with increase of wind speed, and strong destructive force leads to accretion of the number of damaged components. In addition, under the same wind speed, power supply level of *Scenario B* is equal to *Scenario C*. The reason is gas-fired CHPs are not considered in *Scenarios B* and *C*. Therefore, supply level of PS is only related to windstorm intensity in *Scenarios B* and *C* and is not affected by NGS. While power supply level of *Scenario A* is much smaller than that of *Scenario B* (*Scenario C*). For example, power supply levels of *Scenarios A* and *B* (*Scenario C*) are 0.48 and 0.57 when wind speed is 36 m/s. This is because cascading effects aggravate damage caused by the windstorm. That is, EDCs C2 and C3 obtain electric energy from PS to maintain normal operation. However, gas supply to EDCs is reduced to alleviate the shortage of electricity load supply under windstorms. In this case, gas pressure drops in the NGS, which transfers destructiveness of the windstorms to the NGS. Consequently, gas supplies to CHPs are reduced due to reduced gas pressure. Further, reduced output of CHPs exacerbates imbalance of PS. Regarding gas supply levels above Fig. 6(b), although pipelines are not affected by wind speed, gas supply level drops due to the windstorm in *Scenario B*. Because when PS is attacked by the windstorm, power supply level decreases, and electric energy obtained by EDC reduces, thus transferring impact of the windstorm to the NGS. Moreover, gas supply level of *Scenario A* is much smaller than *Scenario B*, which is caused by the cascading effect described above.

It can be seen that due to this cascading effect, the higher the coupling, the smaller the system resilience. It is of great significance to prevent extreme events of IPGS, according to Fig. 7(a). It can be seen that expected electricity energy loss of nodes 1, 2, and 6 near the electrical substation are zeros at the speeds of 31 m/s and 36 m/s. The reason for this is the structure of the electrical substation is designed to be solid to guarantee reliable operation of PS. Corridor 1–2 is underground cable not affected by the windstorm. However, when wind speed increases to 41 m/s, most lines and generators are destroyed, so it is impossible to supply power to node 6. There are significant differences in resilience indicators between different nodes. For example, resilience indicators of nodes 22 and 33 are the largest under all three wind speeds, while resilience indicators of nodes 1 and 2 are the smallest in PS. Furthermore, it can be noted that increase in wind speeds has relatively little impact on ranking of nodal resilience indices in both gas and power systems. This finding can help decision-makers better formulate resilience improvement strategies. For example, decision-makers can harden lines connected to nodes 22 and 33 in advance and set battery storage devices at nodes 22 and 33 to enhance resilience of vulnerable nodes.

Attenuation and recovery ratios for different coupling degrees are shown in Table I.

TABLE I
THE ATTENUATION AND RECOVERY RATIOS OF CASE 2

Wind Speed	Scenario A				Scenario B				Scenario C	
	PS		NGS		PS		NGS		PS	
	R_A	R_R	R_A	R_R	R_A	R_R	R_A	R_R	R_A	R_R
31 m/s	1.05	0.23	1.36	0.06	0.64	0.27	0.82	0.07	0.64	0.27
36 m/s	1.37	0.11	1.53	0.05	0.86	0.19	0.92	0.06	0.86	0.19
41 m/s	1.77	0.09	1.64	0.04	1.42	0.14	0.96	0.05	1.42	0.14

It can be seen from Table I that attenuation ratios increase and recovery ratios decrease with increase of windstorm intensity for all scenarios. With destructive enhancement of windstorms due to the rise in wind speed, system loses partial performance in a short time, which leads to collapse rate increases. On the contrary, the forceful attack damages components, so it takes longer to repair components, and recovery ratios are lower. Moreover, it can be seen from the results of *Scenario A, B, and C* in Table I that with deepening of coupling, system performance declines faster and recovers more slowly.

In order to further verify effectiveness of the proposed method, computation time of integrated resilience evaluation model for different wind speeds is represented, which is shown in Table II.

It can be seen from Table II total time increases a lot with increase of wind speed. The reason is it takes longer to recover to normal operation of IPGS for higher wind speed; that is,

TABLE II
COMPUTATION TIME OF INTEGRATED RESILIENCE EVALUATION MODEL FOR DIFFERENT WIND SPEEDS

Wind Speeds (m/s)	Average computation time Per sample (s)	Total calculation time (s)
31	45.61	55598.59
36	59.53	80067.85
41	76.87	92474.61

T_E is larger. It will take longer to recover to normal operation level. For larger wind speed, that is, T is larger. Therefore, the longer the simulation time to reach T_E. The longest simulation time is 92,474.61 s, which is acceptable for resilience evaluation. Moreover, computation time will increase for large-scale systems. In order to improve computational efficiency, a large-scale system can be decoupled into a series of small systems to accelerate the simulation process through parallel computing [38], [39].

B. Impacts of Windstorms Range on Resilience Evaluation of IPGS

The above analysis is based on windstorms affecting the whole IPGS, but windstorms may affect some areas of IPGs, or different regions are affected by different wind speeds. To discuss impacts of windstorm range on resilience evaluation of IPGS, we compare assessment results of *Case 3*. Taking windstorms with wind speeds of 36 m/s and 41 m/s as an example, there are four scenarios in *Case 3,* which are represented in Table III. Resilience indices for *Case 3* are shown in Fig. 8.

TABLE III
WINDSTORMS RANGE OF CASE 2

Area	Scenario A	Scenario B	Scenario C	Scenario D
Area I	36 m/s	20 m/s	20 m/s	20 m/s
Area II	20 m/s	36 m/s	20 m/s	36 m/s
Area III	20 m/s	20 m/s	36 m/s	41 m/s

As can be seen from Fig. 8, maximum values of L_{EE} and L_{GE} appear in *Scenario A* when windstorms damage only one area; that is, only *Scenarios A* to *C* are compared. The reason is that area I is close to the substation, which is the way to transmit power to area II and area III. When area I is attacked by windstorms, energy supply of PS is threatened, and expected electricity energy is curtailed seriously. Corresponding to it, as mentioned above, reduction of power load increases insufficient power supply to EDCs, resulting in insufficient gas pressure, which makes expected gas energy loss. For the above reasons, both PS and NGS in *Scenario A* crash fastest and recover slowest among the first three scenarios. Besides, compared with area III, there are corridors connecting area I and area II. When energy supply from G1 to a node is affected, it can be supplied by energy from area I and area II. Therefore, minimum values of L_{EE} and L_{GE} appear in *Scenario C*. However, different areas of PS are affected by windstorms at the same time in *Scenario D*. L_{EE} and L_{GE} are increased by 37.8% and 51.7% than in *Scenario A*. Even so, L_{EE} and L_{GE} are generally lower than those in *Case 1*. Besides, the crash is faster, and recovery is slower in

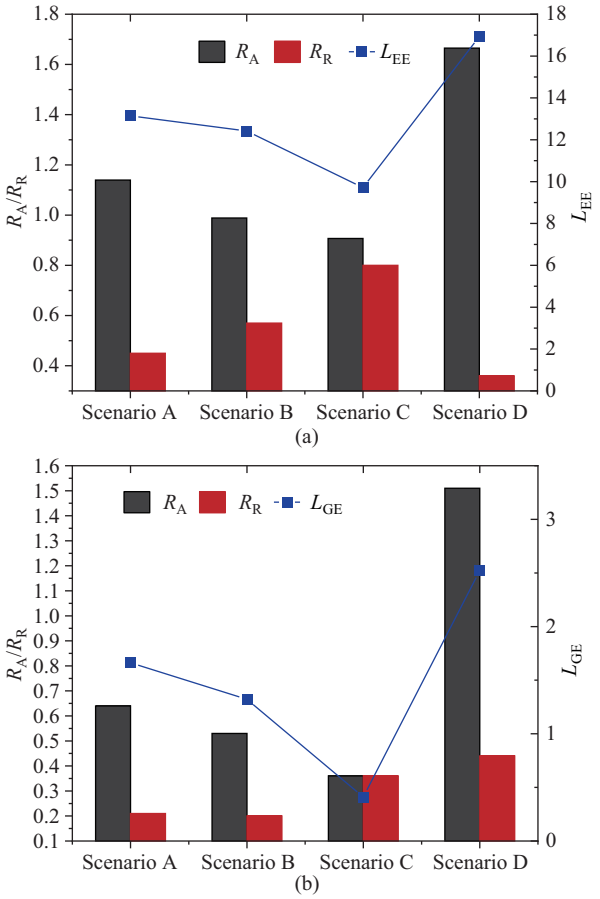

Fig. 8. Resilience indices for *Case 3*. (a) Resilience indices of PS. (b) Resilience indices of NGS.

grid-wide windstorms. It can be seen resilience of the IPGS can be effectively improved by using corresponding resilience improvement means for different regions according to scope of the power grid and location of key equipment.

C. The Impacts of Wind Power Generation Proportion on Resilience Evaluation of IPGS

Cut-out wind speed of WTGS is set to 19∼25 m/s. At the same time, wind speed of a windstorm is larger than 28 m/s according to definition of a windstorm [40]. Therefore, all WTGs are shut down under windstorms. To more comprehensively discuss impacts of WTG capacity on IPGS, we also discuss impacts of the proportion of wind power on IPGS under normal weather and windstorms, in this case, on the basis of the assessment results of *Case 4*. Wind speeds v_1, v_2, and v_3 are set as 10 m/s, 15 m/s, and 31 m/s. There are two scenarios in *Case 4*.

Scenario A: G4 is replaced by WTG of the same capacity, and a P2G device is installed at gas node 19.

Scenario B: G4 and G7 are replaced by WTGs of the same capacity. Two P2G devices are installed at gas nodes 19 and 16, respectively.

L_{EE} and the WTG capacity for *Case 1* and *Case 4* are shown in Fig. 9(a). L_{GE} in NGS for *Case 1* and *Case 4* are shown in Fig. 9(b).

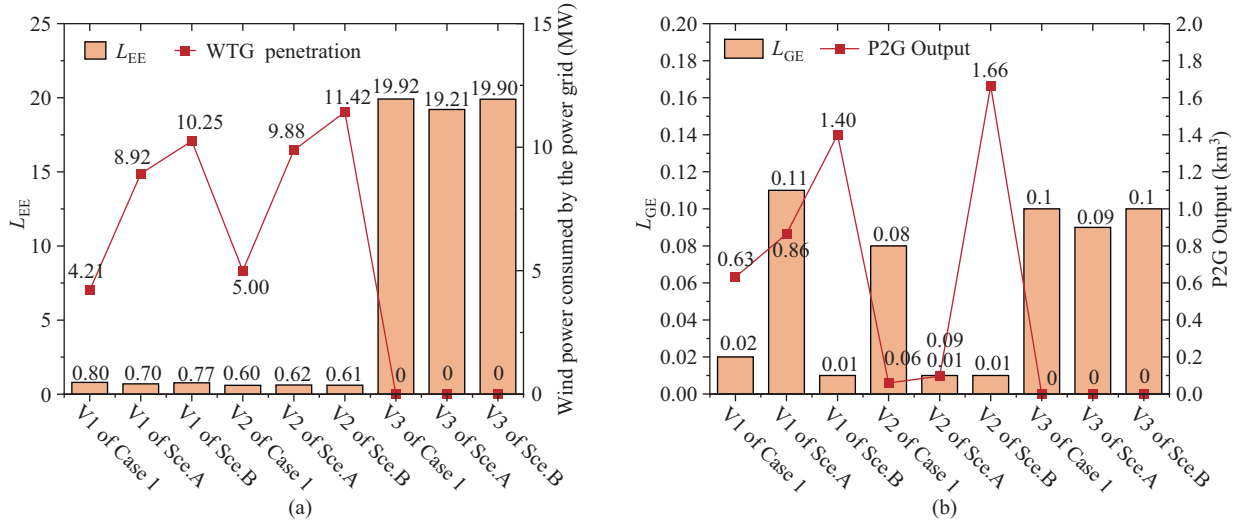

Fig. 9. Simulation results for *Case 1* and *Case 4*. (a) Simulation results of PS. (b) Simulation results of NGS.

Wind power, viewed as an alternative to conventional energy, has received extensive attention. Wind power generation is sensitive to wind speed. Therefore, it is meaningful to discuss influences of WTG capacity on IPGS. Regarding PS above Fig. 9(a), when IPGS has normal weather, that is, wind speed is 10 m/s, and 15 m/s, wind power consumed by the grid grows with increase of their capacity. That is because WTGs are in normal operating states, and increase in WTG capacity raises power generation of WTGs accordingly. Obviously, L_{EE} is small under normal weather. However, L_{EE} is significantly higher than before when wind speed increased to 31 m/s, and fluctuation of L_{EE} for *Case 1* and *Case 4* is minimal. The result is strong wind has damaged the WTG, which is proved by wind power consumed by the power grid in Fig. 9(a). On the other hand, the changing trend of L_{GE} is similar to that of L_{EE}, while values of $L_{\mathrm{GE}}s$ are much smaller than those of $L_{\mathrm{EE}}s$. Because pipelines in the NGS are usually buried underground and are not affected by wind speed, windstorms only destroy PS equipment. Besides, it can be seen above Fig. 9(b) that output of P2Gs is zeros in both two cases at the speed of 31 m/s. The reason is that there is no wind energy abandoned when WTGs are destroyed. Based on the above discussion, when wind speed is 31 m/s, NGS is affected by windstorms to the same extent between *Case 1* and *Case 4*. Through the above comprehensive discussion on impacts of WTG capacity on IPGS, it can be seen that increase of WTG capacity is conducive to consumption of renewable energy under normal weather, but expansion of WTG capacity may greatly reduce resilience of IPGS in extreme events with small probability and large impact. Therefore, the system planner should comprehensively plan WTG capacity according to type and probability of extreme weather suffered by the specific IPGS.

D. Comparison of Evaluation Results with Existing Methods

As outlined in *Section I*, resilience assessment of independent PS and NGS is relatively mature, including literature [10]–[17]. Recently, with deepening of coupling degree between PS and NGS, studies have focused on security resilience evaluation of IPGS, and relevant literature includes [21] and [22]. However, the above references on resilience evaluation of IPGS utilize sequential model. Sequential model takes consideration that one system (*System A*) influences on performance of the other (*System B*), but ignores the reverse effect of *System B* on *System A*. That is, cascading effects between two systems are ignored in sequential model, but the integrated model proposed in this paper considers cascading effects between the two systems. To further verify contributions of the proposed method, evaluation results of independent model, sequential model, and integrated model (the proposed method) are compared. Pipelines in the NGS are usually buried underground and are not affected by windstorms. Therefore, sequential model only destroys equipment of PS and affects operation of NGS through EDCs. Simulation example settings are the same as *Case 1*. Expected electricity energy loss for different resilience assessment models is shown in Fig. 10. Attenuation and recovery ratios for different resilience assessment models are shown in Fig. 11.

It can be seen from Fig. 10(a) that under the same wind speed, L_{EE} of independent model is equal to sequential model. The reason is that reaction of NGS to PS is not considered in sequential model. Therefore, power system is not affected by NGS in independent model and sequential model. Moreover, even though NGS is not directly attacked by the windstorm, insufficient power supply may stop EDCs from functioning when PS is attacked. Therefore, L_{GE} of the sequential model is 1.25, 1.55, and 2.12, corresponding to wind speeds v_1, v_2, and v_3 shown in Fig. 10(b). However, when a disturbance happens in one system, a series of complicated sequences of dependent events may follow in another system closely interconnected through coupling elements between PS and the NGS. Especially under extreme events, cascading effects caused by this coupling relationship are particularly obvious, which can be verified by simulation results of the integrated model. L_{EE} and L_{GE} of integrated model are most among the three resilience evaluation models. The higher the wind

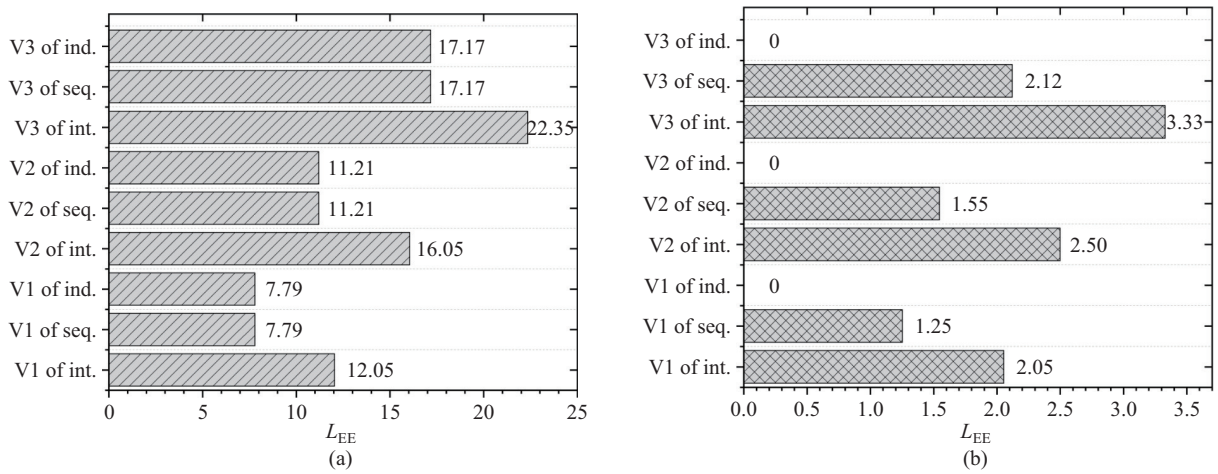

Fig. 10. Expected electricity energy loss for different resilience assessment model. (a) Expected electricity energy loss of the power system. (b) Expected gas energy loss of NGS.

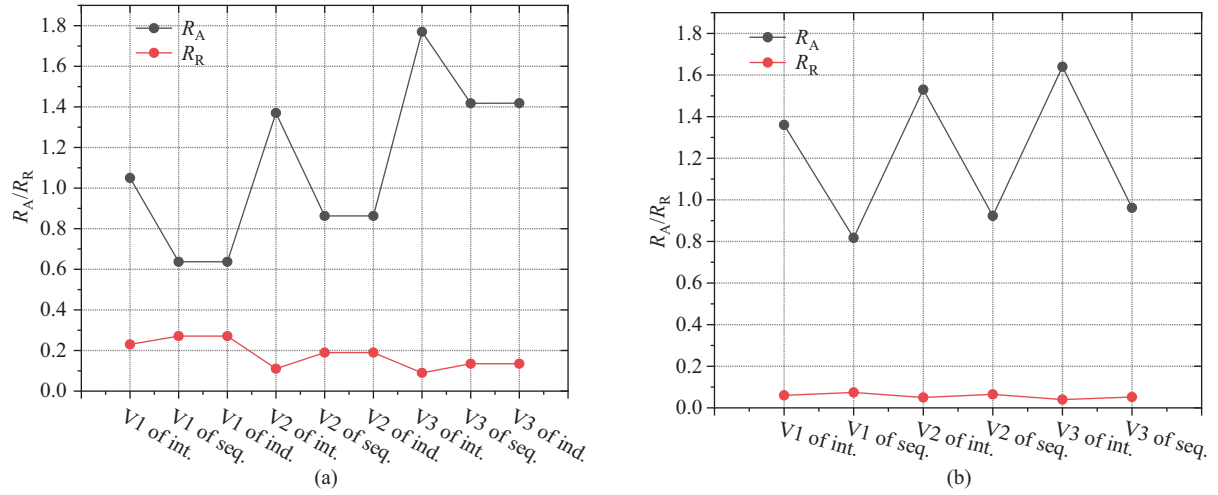

Fig. 11. Attenuation and recovery ratios for different resilience assessment model. (a) Attenuation and recovery ratios of PS. (b) Attenuation and recovery ratios of NGS.

speed, the greater the increase. For example, increase of L_{EE} is 4.26 MW, 4.84 MW, and 5.18 MW when wind speed is v_1, v_2 and v_3, respectively. Regarding attenuation and recovery ratios of PS above Fig. 11(a), R_A and R_R of the sequential model are equal to those of the independent model. Moreover, R_A of integrated model is the most while R_R is the least. Because attenuation ratio of system performance is only related to intensity of extreme weather and resilience of its own in the independent model, as well as in sequential model for PS. However, PS is further worsened due to impact of NGS through coupling components in the integrated model. For example, gas supply to CHPs decreases due to gas load shedding. Based on the above analysis, due to cascading effects between PS and NGS in integrated model, load loss of PS is mostly at the same wind speed, so when recovery strategy is certain, it takes longer to recover. Therefore, R_R is the minimum. Regarding attenuation and recovery ratios of the NGS above Fig. 11(b), due to NGS not being affected by windstorms, R_A and R_R of NGS do not exist in the independent model. Moreover, trends for R_A and R_R of NGS are the same as trends for R_A and R_R of PS, respectively. From the above analysis, it can be concluded when evaluating resilience of IPGS, only evaluating a single system or only considering impact of one system on another while ignoring impact of cascading effects, evaluation results will be too conservative and divorced from the actual situation. Therefore, a resilience model considering cascading effects is necessary.

VI. Conclusion

As the frequency and extent of windstorm events increase, resilience of IPGS needs to be assessed. Time-dependent resilience assessment framework is represented to evaluate IPGS performance levels under windstorms. Four evaluation stages are divided based on a multi-phase performance response curve in the framework. An optimal power flow model is proposed to evaluate resilience of IPGS, which considers cascading effects between PS and NGS. Based on the evaluation model, indicators of nodal resilience considering the relationship with weather elements are utilized to represent the expected level and instantaneous characteristics of resilience in IPGS.

Results of the test systems show the cascading effects increase impacts between NGS and PS, which reduces the resilience of IPGS. Increase in windstorm intensity can dramatically decrease resilience indicators of IPGS. Moreover, windstorm intensity has different effects on resilience of individual nodes. When windstorms are at the regional level, resilience of IPGS varies with the area affected. Obviously, resilience of the IPGS can be effectively improved by using corresponding resilience improvement means for different regions according to the scope destroyed by extreme events of the power grid. Besides, on one hand, increase of WTG capacity improves the utilization of renewable energy. On the other hand, expansion of WTG capacity makes IPGS more threatened and reduces resilience of IPGS under extreme weather. Therefore, planners need to weigh the pros and cons and determine WTG capacity according to the actual situation of the system.

In this paper, an orderly restored strategy is utilized. In fact, repair strategy development for IPGS in recovery phase is related to multiple factors, but is not the focus of this paper. Specific research will be carried out on this subject in the future.

REFERENCES

[1] Q. Peng et al., "Hybrid energy sharing mechanism for integrated energy systems based on the Stackelberg game," in *CSEE Journal of Power and Energy Systems*, vol. 7, no. 5, pp. 911–921, Sep. 2021, doi: 10.17775/CSEEJPES.2020.06500.

[2] Y. Wang, Y. Yang and Q. Xu, "Reliability Assessment for Integrated Power-gas Systems Considering Renewable Energy Uncertainty and Cascading Effects," *CSEE Journal of Power and Energy Systems*, vol. 9, no. 3, pp. 1214–1226, May 2023, doi: 10.17775/CSEEJPES.2022.00740.

[3] B. Zhang, L. Zhang, W. Tang, Z. Wang and C. Wang, "A coordinated restoration method of electric buses and network reconfiguration in distribution systems under extreme events," *CSEE Journal of Power and Energy Systems*, doi: 10.17775/CSEEJPES.2020.04320.

[4] M. Kezunovic, I. Dobson, and Y. M. Dong, "Impact of extreme weather on power system blackouts and forced outages: new challenges," 2008.

[5] X. E. Jiang and Y. S. Wang. (2021, Jul. 21). In addition to the Zhengzhou rainstorm, the world has experienced at least 189 extreme weather events in 2021. [Online]. Available: https://www.thepaper.cn/newsDetail_forward_13675353.

[6] IPCC. (2022). Climate change 2022: mitigation of climate change. [Online]. https://www.ipcc.ch/report/ar6/wg3/downloads/report/IPCC_AR6_WGIII_FullReport.pdf.

[7] W. P. Wang, S. N. Yang, F. Y. Hu, H. E. Stanley, S. He, and M. M. Shi, "An approach for cascading effects within critical infrastructure systems," *Physica A: Statistical Mechanics and its Applications*, vol. 510, pp. 164–177, Nov. 2018, doi: 10.1016/j.physa.2018.06.129.

[8] S. Hosseini, K. Barker, and J. E. Ramirez-Marquez, "A review of definitions and measures of system resilience," *Reliability Engineering & System Safety*, vol. 145, pp. 47–61, Jan. 2016, doi: 10.1016/j.ress.2015.08.006.

[9] J. Z. Lu, J. Guo, Z. Jian, Y. H. Yang, and W. H. Tang, "Resilience assessment and its enhancement in tackling adverse impact of ice disasters for power transmission systems," *Energies*, vol. 11, no. 9, pp. 2272, Aug. 2018, doi: 10.3390/en11092272.

[10] H. B. Liu, R. A. Davidson, and T. V. Apanasovich, "Statistical forecasting of electric power restoration times in hurricanes and ice storms," *IEEE Transactions on Power Systems*, vol. 22, no. 4, pp. 2270–2279, Nov. 2007, doi: 10.1109/TPWRS.2007.907587.

[11] M. Ouyang, L. Dueñas-Osorio, and X. Min, "A three-stage resilience analysis framework for urban infrastructure systems," *Structural Safety*, vol. 36–37, pp. 23–31, May/Jul. 2012, doi: 10.1016/j.strusafe.2011.12.004.

[12] M. Panteli, C. Pickering, S. Wilkinson, R. Dawson, and P. Mancarella, "Power system resilience to extreme weather: fragility modeling, probabilistic impact assessment, and adaptation measures," *IEEE Transactions on Power Systems*, vol. 32, no. 5, pp. 3747–3757, Sep. 2017, doi: 10.1109/TPWRS.2016.2641463.

[13] F. Cadini, G. L. Agliardi, and E. Zio, "A modeling and simulation framework for the reliability/availability assessment of a power transmission grid subject to cascading failures under extreme weather conditions," *Applied Energy*, vol. 185, pp. 267–279, Jan. 2017, doi: 10.1016/j.apenergy.2016.10.086.

[14] M. Ouyang and L. Dueñas-Osorio, "Multi-dimensional hurricane resilience assessment of electric power systems," *Structural Safety*, vol. 48, pp. 15–24, May 2014, doi: 10.1016/j.strusafe.2014.01.001.

[15] G. P. Cimellaro, O. Villa, and M. Bruneau, "Resilience-based design of natural gas distribution networks," *Journal of Infrastructure Systems*, vol. 21, no. 1, pp. 05014005, Mar. 2015, doi: 10.1061/(ASCE)IS.1943-555X.0000204.

[16] Y. T. Ding, S. Chen, Y. L. Zheng, S. L. Chai, and R. Nie, "Resilience assessment of China's natural gas system under supply shortages: a system dynamics approach," *Energy*, vol. 247, pp. 123518, May 2022, doi: 10.1016/j.energy.2022.123518.

[17] P. Hauser, H. Hobbie, and D. Möst, "Resilience in the German natural gas network: modelling approach for a high-resolution natural gas system," in *2017 14th International Conference on the European Energy Market (EEM)*, Dresden, Germany, 2017, pp. 1–6, doi: 10.1109/EEM.2017.7981942.

[18] M. L. Bao, Y. Ding, C. Z. Shao, Y. Yang, and P. Wang, "Nodal reliability evaluation of interdependent gas and power systems considering cascading effects," *IEEE Transactions on Smart Grid*, vol. 11, no. 5, pp. 4090–4104, Sep. 2020, doi: 10.1109/TSG.2020.2982562.

[19] R. Hemmati, H. Mehrjerdi, and S. M. Nosratabadi, "Resilience-oriented adaptable microgrid formation in integrated electricity-gas system with deployment of multiple energy hubs," *Sustainable Cities and Society*, vol. 71, pp. 102946, Aug. 2021, doi: 10.1016/j.scs.2021.102946.

[20] Y. T. Xu, S. S. Chen, S. M. Tian, and F. X. Gong, "Demand management for resilience enhancement of integrated energy distribution system against natural disasters," *Sustainability*, vol. 14, no. 1, pp. 5, Dec. 2021, doi: 10.3390/su14010005.

[21] H. J. Zhang, T. Y. Zhao, P. Wang, and S. H. Yao, "Power system resilience assessment considering of integrated natural gas system," in *IET International Conference on Resilience of Transmission and Distribution Networks (RTDN 2017)*, Birmingham, UK, 2017, pp. 1–7, doi: 10.1049/cp.2017.0334.

[22] H. J. Zhang, P. Wang, S. H. Yao, X. C. Liu, and T. Y. Zhao, "Resilience assessment of interdependent energy systems under hurricanes," *IEEE Transactions on Power Systems*, vol. 35, no. 5, pp. 3682–3694, Sep. 2020, doi: 10.1109/TPWRS.2020.2973699.

[23] E. B. Watson and A. H. Etemadi, "Modeling electrical grid resilience under hurricane wind conditions with increased solar and wind power generation," *IEEE Transactions on Power Systems*, vol. 35, no. 2, pp. 929–937, Mar. 2020, doi: 10.1109/TPWRS.2019.2942279.

[24] M. L. Bao, Y. Ding, M. S. Sang, D. Q. Li, C. Z. Shao, and J. Y. Yan, "Modeling and evaluating nodal resilience of multi-energy systems under windstorms," *Applied Energy*, vol. 270, pp. 115136, Jul. 2020, doi: 10.1016/j.apenergy.2020.115136.

[25] A. F. Mensah, "Resilience assessment of electric grids and distributed wind generation under hurricane hazards," Ph.D. dissertation, department, Rice University, Houston, TX, 2015.

[26] *Code for Design of 20kV and Below Substations*, GB 50053–2013, 2014.

[27] Code for Design of Small Fossil Fired Power Plant, GB 50049–2011, 2011.

[28] S. Rose, P. Jaramillo, M. J. Small, and J. Apt, "Quantifying the hurricane catastrophe risk to offshore wind power," *Risk Analysis*, vol. 33, no. 12, pp. 2126–2141, Dec. 2013, doi: 10.1111/risa.12085.

[29] W. H. Tang, Y. H. Yang, Y. J. Li, J. Z. Lu, and Q. H. Wu, "Investigation on resilience assessment and enhancement for power transmission systems under extreme meteorological disasters," *Proceedings of the CSEE*, vol. 40, no. 7, pp. 2244–2254, Apr. 2020, doi: 10.13334/j.0258-8013.pcsee.182191.

[30] B. J. Li, H. W. Qi, J. Y. Fu, Z. H. Gao, and L. Guo, "Analysis on the impact of extreme weather on new energy operation," *Jilin Electric Power*, vol. 50, no. 1, pp. 10–13, Feb. 2022, doi: 10.16109/j.cnki.jldl.2022.01.002.

[31] H. Y. Yuan, F. X. Li, Y. L. Wei, and J. X. Zhu, "Novel linearized power flow and linearized OPF models for active distribution networks with application in distribution LMP," *IEEE Transactions on Smart Grid*, vol. 9, no. 1, pp. 438–448, Jan. 2018, doi: 10.1109/TSG.2016.2594814.

[32] A. Mehrtash, P. Wang, and L. Goel, "Reliability evaluation of power systems considering restructuring and renewable generators," *IEEE Transactions on Power Systems*, vol. 27, no. 1, pp. 243–250, Feb. 2012, doi: 10.1109/TPWRS.2011.2161350.

[33] M. Panteli, P. Mancarella, D. N. Trakas, E. Kyriakides, and N. D. Hatziargyriou, "Metrics and quantification of operational and infrastructure resilience in power systems," *IEEE Transactions on Power Systems*, vol. 32, no. 6, pp. 4732–4742, Nov. 2017, doi: 10.1109/TPWRS.2017.2664141.
[34] C. Wang and M. H. Nehrir, "Analytical approaches for optimal placement of distributed generation sources in power systems," *IEEE Transactions on Power Systems*, vol. 19, no. 4, pp. 2068–2076, Nov. 2004, doi: 10.1109/TPWRS.2004.836189.
[35] D. De Wolf and Y. Smeers, "The gas transmission problem solved by an extension of the simplex algorithm," *Management Science*, vol. 46, no. 11, pp. 1454–1465, Nov. 2000, doi: 10.1287/mnsc.46.11.1454.12087.
[36] S. An, Q. Li, and T. W. Gedra, "Natural gas and electricity optimal power flow," in *2003 IEEE PES Transmission and Distribution Conference and Exposition*, Dallas, TX, USA, 2003, pp. 138–143, doi: 10.1109/TDC.2003.1335171.
[37] K. A. Pambour, B. C. Erdener, R. Bolado-Lavin, and G. P. J. Dijkema, "Development of a simulation framework for analyzing security of supply in integrated gas and electric power systems," *Applied Sciences*, vol. 7, no. 1, pp. 47, Jan. 2017.
[38] D. A. Alves, L. C. P. da Silva, C. A. Castro, and V. F. da Costa, "Continuation fast decoupled power flow with secant predictor," *IEEE Transactions on Power Systems*, vol. 18, no. 3, pp. 1078–1085, Aug. 2003, doi: 10.1109/TPWRS.2003.814892.
[39] Q. D. Meng, S. Zhang, B. X. Li, X. Li, and G. Q. Li, "Fast decoupling based parallel computing method for continuation power flow in power system," *Proceedings of the CSU-EPSA*, vol. 33, no. 7, pp. 41–48, Jul. 2021, doi: 10.19635/j.cnki.csu-epsa.000742.
[40] "Wind grade table", *Qinghai Agro-Technology Extension*, vol. 2022, no. 3, pp. 55.

Yucui Wang is currently working toward the Ph.D. degree in the School of Cyber Science and Engineering, Southeast University, Nanjing, China. Her research interests include reliability analysis of the integrated energy system, and power system operation.

Yongbiao Yang received the B.S. degree in Electrical Engineering from Southwest Jiaotong University, China, in 2001, the M.S. degree in Energy and Power Engineering from Nanjing University of Science and Technology in 2013. He is currently a Senior Engineer at Southeast University. His research interests include reliability analysis, demand response and integrated energy system.

Qingshan Xu received the B.S. degree from Southeast University, Nanjing, China, in 2000, the M.S. degree from Hohai University, Nanjing, in 2003, and the D.E. degree from Southeast University in 2006, all in Electrical Engineering. He is currently a full Professor of Electrical Engineering School of Southeast University, China. His research interests include renewable energy, power system operation and control and etc.